An Optical Clearing Technique for Plant Tissues Allowing Deep Imaging and Compatible with Fluorescence Microscopy[1][W][OPEN]

Cherish A. Warner, Meredith L. Biedrzycki, Samuel S. Jacobs, Randall J. Wisser, Jeffrey L. Caplan*, and D. Janine Sherrier*

Delaware Biotechnology Institute (C.A.W., S.S.J., J.C., D.J.S.) and Departments of Biological Sciences (C.A.W., M.L.B., S.S.J., J.C., D.J.S.); and Plant and Soil Sciences (M.L.B., R.J.W., J.C., D.J.S.), University of Delaware, Newark, Delaware 19717–1303

We report on a nondestructive clearing technique that enhances transmission of light through specimens from diverse plant species, opening unique opportunities for microscope-enabled plant research. After clearing, plant organs and thick tissue sections are amenable to deep imaging. The clearing method is compatible with immunocytochemistry techniques and can be used in concert with common fluorescent probes, including widely adopted protein tags such as GFP, which has fluorescence that is preserved during the clearing process.

Fluorescence-based microscopy and three-dimensional imaging have revolutionized plant science research, leading to unique insights into phenotypic variation (Meijón et al., 2014), plant-microbe interactions (Dagdas et al., 2012), and gene expression patterns (Truernit et al., 2008). However, the potential of these technologies to help tackle a range of fundamental questions in plant biology has not been fully realized because of limitations caused by plants' intrinsic properties and current methods used for sample preparation. The transmission of light through plant cells is impeded by the heterogeneous refractive indices of the cell wall and cytoplasm, and light is absorbed by pigments. In addition, the fluorescence of pigments and aromatic molecules further reduces the signal-to-noise ratio in images. Collectively, these intrinsic properties restrict the imaging depth for plant samples to approximately 30 μm, representing the distance of only a few layers of cells, a depth much lower than the theoretical limits of modern confocal microscopes and result in poor image quality (Feijó and Moreno, 2004; Paddock and Eliceiri, 2014).

To visualize internal plant structures, samples may be sectioned mechanically or processed using a clearing agent before imaging. Sectioning is labor and time intensive and can be complicated by the loss or damage of structures. It also requires alignment of serial images for interpretation within the context of the whole tissue, and this can also lead to inaccuracies in the representation of a specimen. Alternatively, solvents, such as ethanol, are frequently used to clear thick tissue samples (Phillips and Hayman, 1970; Gardner, 1975). Although this approach yields greater tissue transparency and light transmission, it unfortunately also results in the extraction of cellular constituents and the disruption of subcellular structures. Chloral hydrate preserves cellular features better than many other solvents (Lersten, 1986), but its alternative use as a sedative or hypnotic drug prevents widespread adoption in routine laboratory studies.

In the past few years, rapid advances in mammalian tissue clearing techniques have facilitated microscopic analysis of whole tissues and intact organisms (Hama et al., 2011; Chung et al., 2013; Ke et al., 2013). Treatment of whole mouse embryos with one such reagent facilitated microscopic analysis of entire neuronal networks tagged with GFP (Hama et al., 2011). The goal of this work was to develop and fine tune a method to facilitate deep-tissue imaging of intact plant organs or whole plants. Specifically, we aimed to develop an approach to retain fine cellular features in specimens, closely match the refractive indices of plant tissues, enhance light transmission through the sample, and preserve the ability to use common fluorescent stains and proteins. The plant-tissue clearing agent presented here overcomes all the major obstacles that have limited plant imaging to date, and it is, therefore, of broad use to the plant scientific community.

[1] This work was supported by the National Science Foundation (grant nos. NSF–IOS–1127076 to R.J.W., NSF–IOS–1127155 to D.J.S., and NSF–IOS–0923668 to D.J.S.) and the National Institutes of Health (grant no. 5R01GM097587 to J.L.C.).

* Address correspondence to jcaplan@udel.edu and sherrier@dbi.udel.edu.

The author responsible for distribution of materials integral to the findings presented in this article in accordance with the policy described in the Instructions for Authors (www.plantphysiol.org) is: D. Janine Sherrier (sherrier@dbi.udel.edu).

C.A.W., M.L.B., and S.S.J. performed most of the experiments; S.S.J. provided technical assistance to C.A.W.; C.A.W. and M.L.B. designed the experiments and analyzed the data; J.L.C. and D.J.S. conceived the project collaboratively; and R.J.W., J.L.C., and D.J.S. supervised and finalized the writing.

[W] The online version of this article contains Web-only data.

[OPEN] Articles can be viewed online without a subscription.

www.plantphysiol.org/cgi/doi/10.1104/pp.114.244673

RESULTS

Clearing efficacy in photosynthetic and root-derived samples from monocot and dicot species was assessed in preserved samples treated with clearing solution. The formulation developed for this study was highly effective at clearing leaves and roots of all tested plant species, including Arabidopsis (*Arabidopsis thaliana*), *Medicago truncatula*, pea (*Pisum sativum*), *Nicotiana benthamiana*, and maize (*Zea mays*; Supplemental Fig. S1). Clearing substantially increased tissue transparency compared with untreated tissue (Fig. 1). The method cleared specimens optically in as little as 1 to 3 weeks, making them ready for staining and complete traverse imaging

Samples of mature monocotyledonous leaves became transparent after treatment (Fig. 1A; Supplemental Fig. S1), even in areas with thickened secondary wall development, such as the veins. Similarly, intact samples from dicotyledonous plants, such as leaves and root nodules from pea, became transparent after treatment (Fig. 1, C and D; Supplemental Fig. S1, G and F).

We assessed the depth of imaging achievable in cleared tissues using thick sections from root nodules.

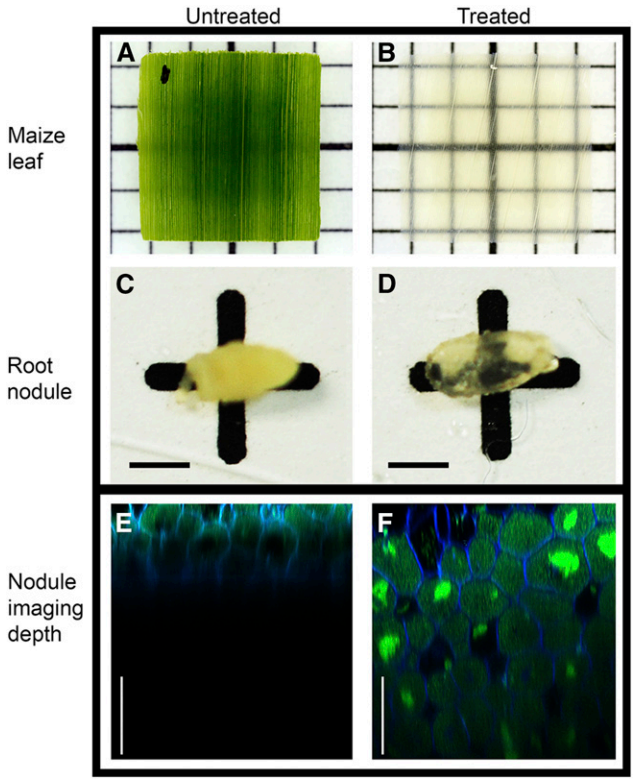

Figure 1. Tissue clearing performance and imaging. Photos of a maize leaf punch and intact pea root nodule taken before (A and C) and after (B and D) treatment with clearing solution. Grid scale = 15 mm in A and B. Bars = 500 μm in C and D. Depth of imaging achievable in the *z* axis of untreated and treated nodule tissue (E and F). Root nodule tissue was stained with the cellulose stain Calcofluor White (blue) and nucleic acid stain SYTO13 (green) and imaged using a multiphoton confocal microscope. Bars = 100 μm.

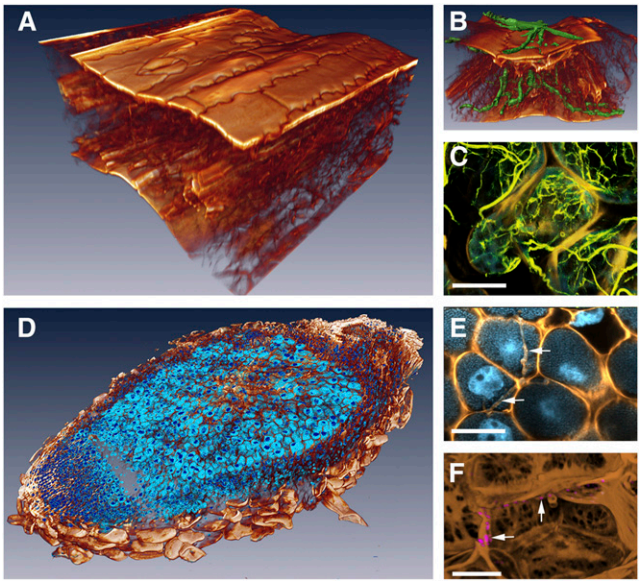

Figure 2. Three-dimensional reconstructions of cleared specimens and compatibility with fluorescent markers. A and B, Three-dimensional rendering of a cleared maize leaf (approximately 200 μm thick). A, Cell walls were stained with Calcofluor White (brown). B, Fungal hyphae was stained with Alexa Fluor 594 wheat germ agglutinin (green). C, Three-dimensional maximum intensity projection of *N. benthamiana* leaf expressing protein marker mTalin-Citrine labeling actin filaments (green). D to F, Pea root nodules stained with Calcofluor White (brown) and SYTO13 (blue). D, A 200-μm-thick three-dimensional rendering reconstructed from multiple *z* stacks. E, An infection thread traversing multiple cells (arrows). F, Cell walls with cellulose microfibril lattice structures (brown) labeled with anti-β-1,3-glucan and Alexa Fluor 568 antibodies (arrows; magenta). Bars = 20 μm in C, E, and F.

Cleared samples and uncleared controls were stained with SYTO13 and Calcofluor White and imaged using a multiphoton confocal microscope and a 25×/0.8 LD LCI PlanApochromat multiimmersion lens mounted with 30% (v/v) glycerol. Tissue clearing increased the depth of imaging by more than 3-fold compared with untreated tissue, with the depth of the *z* axis more than 350 μm in treated samples compared with 100 μm in untreated samples (Fig. 1, E and F).

The notable increase in depth of imaging after clearing allowed for three-dimensional analysis of multiple cell layers in different specimens. Transverse optical images of the entire thickness of a cleared maize leaf were rendered by *z*-stack reconstruction using Huygen's Professional deconvolution and Amira three-dimensional visualization software (Fig. 2, A and B). This analysis allowed cell layers, cell junctions, and tissue structures to be visualized in the three-dimensional models, highlighting the mesophyll and vasculature structural features through the maize leaf (Fig. 2A; Supplemental Movie S1). Furthermore, the spatial relationship of these structures to a fungal pathogen, *Cochliobolus heterostrophus*, could be determined from whole-thickness samples (Fig. 2B). Using the same rendering methods, an optical section (200-μm thick) was collected and reassembled

from the central zone of an intact pea root nodule (Fig. 2D; Supplemental Movie S2). Key features could be analyzed without physical disruption of the intricate association between pea and *Rhizobium leguminosarum* bv viciae, including infection threads traversing multiple cells (Fig. 2E).

To evaluate the preservation of subcellular features and the compatibility of clearing with the use of fluorescent marker proteins, we cleared samples of *N. benthamiana* leaves expressing a fluorescent marker protein. The fluorescent property of the marker for actin, mTalin (Kost et al., 1998) tagged with the yellow GFP variant Citrine, was retained, allowing for visualization of both fine and thick actin bundles (Fig. 2C; Supplemental Figs. S2 and S3). Consistent with the results reported from studies using standard microscopic techniques with fluorescent reporter proteins in fixed tissues, the marker retained fluorescence after fixation (Supplemental Fig. S2; Knapp et al., 2012). Furthermore, the distribution and fluorescence of the actin marker from cleared fixed tissue were comparable with those of fixed tissue (Supplemental Fig. S3). The preservation of the marker protein fluorescence in addition to fine subcellular structure opens the possibility to study protein distribution within every cell type using intact specimens treated with the clearing solution.

Although fluorescent tags are commonly used to determine subcellular distribution of proteins, immunocytochemical methods are used to visualize the distribution of proteins and nonproteinaceous cellular constituents. To determine if immunocytochemical methods could be used as well, cleared nodule tissues were probed with anti-β-1,3-glucan antibodies using standard methods (Catalano et al., 2007) to determine the distribution of callose. Cleared samples were washed to remove clearing solution, immunolabeled, and subsequently reinfiltrated with the clearing solution for imaging. As expected, callose was detected on the cell walls within the central zone of nodule tissue (Fig. 2F, arrows). Although clearing did not result in a measureable increase in penetration of a large antibody probe into this tissue, it is possible that antibody penetration could be enhanced using established methods (Blancaflor et al., 2001; Harrison et al., 2002). These results, however, unequivocally show compatibility of clearing with immunolocalization methods and the preservation of fluorescent protein tags.

DISCUSSION

In conclusion, our goal was to show the potential range of applications when using this clearing technique and provide a guide for researchers to achieve clarity and imaging depth for their samples. This advancement in optical clearing uniquely enables deep, complete traverse imaging of plant specimens using a broadly accessible formulation that is compatible with fluorescent stains, fluorescent protein tags, and immunolabeling, opening a range of unique possibilities for microscopic investigation in plant biology.

MATERIALS AND METHODS

Sample Preparation and Clearing

Maize Leaf

Maize (*Zea mays*) infected with *Cochliobolus heterostrophus* was harvested 3 d postinoculation directly into 2% (v/v) glutaraldehyde, 2% (w/v) paraformaldehyde, and 0.05% (v/v) Triton X-100 in phosphate-buffered saline (PBS; pH 7.4). Samples were a gift from Peter J. Balint-Kurti at USDA-ARS. Using 15 mm^2 of excised leaf, samples were treated with 10% (w/v) KOH for 8 h at room temperature, rinsed three times in PBS for 5 min, and subsequently stained with 1.09 mM Calcofluor White MR2 (Sigma-Aldrich); for imaging of fungal hyphae, they were incubated simultaneously with 0.026 mM Alexa Fluor 594 conjugate of wheat (*Triticum aestivum*) germ agglutinin (Life Technologies) for 5 d. Samples were rinsed three times in PBS for 5 min and transferred to clearing solution containing 6 M urea, 30% (v/v) glycerol, and 0.1% (v/v) Triton X-100 in sterile water for 48 h with gentle rotation at room temperature.

Pea Root Nodule

Nodules infected with *Rhizobium leguminosarum* bv *viciae* wild-type strain 3841 were grown using established methods (Vedam et al., 2004). At 21 d postinoculation, nodules were harvested and fixed overnight in 4% paraformaldehyde in 80 mM PIPES (pH 7.0) with gentle rotation at 4°C. Samples were then rinsed three times for 5 min in 80 mM PIPES (pH 7.0) and incubated in 6 M urea, 30% (v/v) glycerol, and 0.1% (v/v) Triton X-100 clearing solution containing 80 mM PIPES (pH 7) for 1 to 3 weeks at 4°C with rotation. The samples were checked at weekly intervals until the desired degree of transparency was achieved.

Medicago truncatula and Pea Leaves

Intact *M. truncatula* leaves or samples excised from the middle of pea (*Pisum sativum*) leaves were harvested from 3-week-old plants grown according to established methods (Vedam et al., 2004; Catalano et al., 2007) and fixed overnight in 4% (w/v) paraformaldehyde in 80 mM PIPES (pH 7.0) with gentle rotation at 4°C. Samples were then rinsed three times for 5 min in 80 mM PIPES (pH 7) and incubated in the clearing solution above for 1 to 3 weeks at 4°C with gentle rotation. The samples were checked at weekly intervals until the desired degree of transparency was achieved.

Nicotiana benthamiana Leaves

Leaves from *N. benthamiana* plant line 59-8-3 were infiltrated with *Agrobacterium tumefaciens* encoding the fluorescent actin marker mTalin tagged with Citrine (Kost et al., 1998; Caplan et al., 2008). After 36 h, leaves were harvested directly into 4% (w/v) paraformaldehyde in 60 mM PIPES, 25 mM HEPES, 10 mM EGTA, and 2 mM $MgCl_2$ (pH 6.9; PHEM) and fixed at 4°C overnight with gentle rotation. Samples were then cleared with 6 M urea, 30% (v/v) glycerol, and 0.1% (v/v) Triton X-100 in PHEM for 1 to 3 weeks at 4°C with gentle rotation. The samples were checked at weekly intervals until the desired degree of transparency was achieved.

Immunolabeling of Cleared Nodule Tissue

Medial hand sections of nodules were cleared as described and rinsed three times for 5 min with 80 mM PIPES, 5 mM $MgSO_4$, and 10 mM EGTA (pH 7.0; Harrison et al., 2002). To facilitate antibody infiltration, samples were incubated in 0.1% (w/v) bovine serum albumin fraction V, 1.0% (w/v) cellulase, and 0.01% (w/v) pectolysase digesting enzymes (Karlan Research Corp.) in 80 mM PIPES, 5 mM $MgSO_4$, and 10 mM EGTA (pH 7.0) for 20 min. Nodules were rinsed three times with Tris-buffered saline (TBS) for 5 min per rinse and transferred to 3% (w/v) bovine serum albumin fraction V and 1% (v/v) normal goat serum in TBS (pH 7.4; blocking buffer) for 1 h. Samples were transferred to an antibody solution of 1:1,000 anti-β-1,3-glucan antibodies (BioSupplies) in fresh blocking buffer, incubated for 2 h, rinsed three times in TBS with 0.05% (v/v) Tween 20 and one time with TBS for 5 min, and transferred to a 1:500 dilution of Alexa Fluor 568 goat anti-mouse IgG_1 (Molecular Probes) in blocking solution for 1 h. Samples were rinsed with TBS three times for 5 min and then again with 80 mM PIPES (pH 7) for 5 min and transferred back into the clearing solution at room temperature.

Data Acquisition and Fluorescent Microscopy

Depth of Imaging and Image Acquisition Using Confocal Microscopy

Cleared *N. benthamiana* leaves expressing mTalin-Citrine were stained with Calcofluor White MR2 (1.09 mM) for 1 h before imaging. Immunolabeled nodules were also stained with 0.005 mM SYTO13 and 1.09 mM Calcofluor White MR2 for 1 h before imaging. Tissues were placed in a single-well Nunc Lab-Tek II Chambered Coverglass system in fresh clearing solution. *z* Stacks of samples were collected using a Zeiss LSM 510 NLO multiphoton confocal microscope. For three-dimensional renderings of maize leaf and root nodule, *z* intervals were 0.611 and 1.2 μm, respectively. For samples used to compare the impact of fixation and tissue clearing on morphology and fluorescence, live samples were imaged, removed from the Nunc chamber for 30 min fixation at room temperature in 4% (w/v) paraformaldehyde in PHEM, and reimaged. To evaluate the impact of the clearing treatment, fixed tissues were imaged and subsequently cleared for 3 weeks (Supplemental Fig. S3). Images in Supplemental Figures S2 and S3 were acquired using a Zeiss LSM 710 confocal microscope. Lenses used for image acquisition included a 40× LD C-Apochromat water lens (numerical aperture [NA] of 1.1; working distance of 0.62 mm) and a 25× LD LCI PlanApochromat multiimmersion lens using 30% (v/v) glycerol as mounting medium (NA of 0.80; working distance of 0.57 mm).

Image Processing and Three-Dimensional Visualization

z Stacks were deconvolved using Huygen's Professional deconvolution software, version 3.4.0p1 (Scientific Volume Imaging). The confocal channels representing specific emission spectra were separated and deconvolved using the classical maximum likelihood estimation with the following parameters changed: quality change threshold = 0.01%, maximum iteration = 40, and signal-to-noise per channel values = 5, 20, 20, and 20. The data sets were then imported into Amira 3D visualization software, version 5.4.5 (FEI Visualization Sciences Group). Three-dimensional renderings were created using a volume-rendering visualization technique (Voltex) based on the emission-absorption of light of every voxel in the stack. Different color maps were then assigned to each channel to distinguish individual fluorescent signals.

Imaging of Additional Cleared Tissue Types

Maize leaf samples and intact pea root nodules in 80 mM PIPES were imaged against a patterned background before clearing. Samples were then imaged against the same background seen in Figure 1, A to D, after 3 weeks of clearing. Samples shown in Supplemental Figure S1 of leaves from *M. truncatula*, *N. benthamiana*, Arabidopsis (*Arabidopsis thaliana*), and pea were photographed using the same technique as the maize leaf and root nodule.

Notes on Clearing

During the preparation of the clearing solution, urea is slow to dissolve. If gentle heat is used to speed dissolution, care should be taken to prevent the breakdown of urea into isocyanate. The solvent should be stirred with a heavy magnetic bar, and the temperature should never exceed 30°C. The solution should be removed from the heat source immediately on urea dissolution. The use of a multiimmersion lens is recommended to achieve maximum optical gains, because both the NA of the lens and the refractive index of a glycerol-based mounting medium can be adjusted to match the refractive index of the clearing solution precisely.

Supplemental Data

The following materials are available in the online version of this article.

Supplemental Figure S1. Clearing effects in monocot and dicot leaf tissues.

Supplemental Figure S2. Actin distribution in live and fixed *N. benthamiana*.

Supplemental Figure S3. Actin distribution in fixed and cleared *N. benthamiana*.

Supplemental Movie S1. Maize leaf three-dimensional reconstruction.

Supplemental Movie S2. Three-dimensional optical slice through central nodule tissue.

ACKNOWLEDGMENTS

We thank Amutha Kumar and Dr. Savithramma Dinesh-Kumar for providing *N. benthamiana* plant samples and the laboratory of Peter J. Balint-Kurti (U.S. Department of Agriculture, Agricultural Research Service) for providing maize infected with *C. heterostrophus*.

Received June 6, 2014; accepted October 19, 2014; published October 24, 2014.

LITERATURE CITED

Blancaflor EB, Zhao L, Harrison MJ (2001) Microtubule organization in root cells of *Medicago truncatula* during development of an arbuscular mycorrhizal symbiosis with *Glomus versiforme*. Protoplasma **217:** 154–165

Caplan JL, Mamillapalli P, Burch-Smith TM, Czymmek K, Dinesh-Kumar SP (2008) Chloroplastic protein NRIP1 mediates innate immune receptor recognition of a viral effector. Cell **132:** 449–462

Catalano CM, Czymmek KJ, Gann JG, Sherrier DJ (2007) *Medicago truncatula* syntaxin SYP132 defines the symbiosome membrane and infection droplet membrane in root nodules. Planta **225:** 541–550

Chung K, Wallace J, Kim SY, Kalyanasundaram S, Andalman AS, Davidson TJ, Mirzabekov JJ, Zalocusky KA, Mattis J, Denisin AK, et al (2013) Structural and molecular interrogation of intact biological systems. Nature **497:** 332–337

Dagdas YF, Yoshino K, Dagdas G, Ryder LS, Bielska E, Steinberg G, Talbot NJ (2012) Septin-mediated plant cell invasion by the rice blast fungus, *Magnaporthe oryzae*. Science **336:** 1590–1595

Feijó JA, Moreno N (2004) Imaging plant cells by two-photon excitation. Protoplasma **223:** 1–32

Gardner RO (1975) An overview of botanical clearing technique. Stain Technol **50:** 99–105

Hama H, Kurokawa H, Kawano H, Ando R, Shimogori T, Noda H, Fukami K, Sakaue-Sawano A, Miyawaki A (2011) Scale: a chemical approach for fluorescence imaging and reconstruction of transparent mouse brain. Nat Neurosci **14:** 1481–1488

Harrison MJ, Dewbre GR, Liu J (2002) A phosphate transporter from *Medicago truncatula* involved in the acquisition of phosphate released by arbuscular mycorrhizal fungi. Plant Cell **14:** 2413–2429

Ke MT, Fujimoto S, Imai T (2013) SeeDB: a simple and morphology-preserving optical clearing agent for neuronal circuit reconstruction. Nat Neurosci **16:** 1154–1161

Knapp E, Flores R, Scheiblin D, Scheiblin D, Modla S, Czymmek K, Czymmek K, Yusibov V (2012) A cryohistological protocol for preparation of large plant tissue sections for screening intracellular fluorescent protein expression. Biotechniques **52:** 31–37

Kost B, Spielhofer P, Chua NH (1998) A GFP-mouse talin fusion protein labels plant actin filaments *in vivo* and visualizes the actin cytoskeleton in growing pollen tubes. Plant J **16:** 393–401

Lersten NR (1986) Modified clearing method to show sieve tubes in minor veins of leaves. Stain Technol **61:** 231–234

Meijón M, Satbhai SB, Tsuchimatsu T, Busch W (2014) Genome-wide association study using cellular traits identifies a new regulator of root development in Arabidopsis. Nat Genet **46:** 77–81

Paddock SW, Eliceiri KW (2014) Laser scanning confocal microscopy: history, applications, and related optical sectioning techniques. Methods Mol Biol **1075:** 9–47

Phillips JM, Hayman DS (1970) Improved procedures for clearing roots and staining parasitic and vesicular-arbuscular mycorrhizal fungi for rapid assessment of infection. Trans Br Mycol Soc **55:** 158–161

Truernit E, Bauby H, Dubreucq B, Grandjean O, Runions J, Barthélémy J, Palauqui JC (2008) High-resolution whole-mount imaging of three-dimensional tissue organization and gene expression enables the study of phloem development and structure in *Arabidopsis*. Plant Cell **20:** 1494–1503

Vedam V, Haynes JG, Kannenberg EL, Carlson RW, Sherrier DJ (2004) A *Rhizobium leguminosarum* lipopolysaccharide lipid-A mutant induces nitrogen-fixing nodules with delayed and defective bacteroid formation. Mol Plant Microbe Interact **17:** 283–291